Supporting Information

An et al. 10.1073/pnas.1607506113

1. Processing and Testing Details

The $Pd_{82}Si_{18}$ alloy was prepared by inductively melting high-purity elements (Pd, 99.95%; Si, 99.9999%) in quartz tubes under a high-purity argon atmosphere. The alloy ingot was fluxed with B_2O_3 in a quartz tube under a high-purity argon atmosphere at 1,200 °C for 16 h. Amorphous rods 1 mm in diameter were prepared by furnace-melting the fluxed ingots in round quartz capillaries with 100-μm-thick walls under a high-purity argon atmosphere, followed by rapid water-quenching.

The $Cu_{46}Zr_{54}$ alloy was prepared by arc-melting high-purity elements [Zr, 99.9% (crystal bar; Hf, 0.028% wt; O, 110 ppm wt); Cu, 99.995%] over a water-cooled copper hearth under a titanium-gettered argon atmosphere. Amorphous rods 1 mm in diameter were prepared by arc-melting the alloy ingots under a titanium-gettered argon atmosphere, followed by suction-casing into a copper mold.

Three-point bending tests of 1-mm amorphous rods of $Pd_{82}Si_{18}$ and $Cu_{46}Zr_{54}$ were performed at room temperature on a screw-driven Instron testing machine (Instron). A bending fixture with a span distance of 6.35 mm was used. Strain was recorded using a linear variable displacement transducer.

2. Simulation Details and Analysis Methods

We use the embedded-atom-method potential developed to describe the interactions for Zr-Cu and Pd-Si (28). MD simulations were performed on $Cu_{46}Zr_{54}$ and $Pd_{82}Si_{18}$ MGs using large-scale atomic/molecular massively parallel simulator (LAMMPS) (29), with periodic boundary condition applied for all three dimensions. Simulation cell sizes at ambient conditions are 83.27 and 78.21 Å for $Cu_{46}Zr_{54}$ and $Pd_{82}Si_{18}$, respectively. The samples were melted and equilibrated at 2,000 K for 1 ns with a time step 1.0 fs and quenched into the glassy state (300 K) at cooling rates of 1.0×10^{12} K s^{-1}. Isothermal–isobaric (NPT) and canonical (NVT) ensembles are applied in the simulations using the Nose–Hoover thermostat (damping constant 100 fs) and barostat (damping constant 1,000 fs) to adjust temperature and pressures. At room temperature, the system is hydrostatically expanded along three directions with a constant rate of 2.0×10^8/s by scaling the atomic coordination of all atoms at each MD step. In shear deformation, the system is sheared under a constant engineering strain rate of 1.0×10^{10} s^{-1}.

We use a grid-based method (25) to characterize the nanovoid in the deformation simulations. From a radial distribution function, we get nearest-neighbor distances (R_{nn}) equal to 3.85 and 3.53 Å for $Pd_{82}Si_{18}$ and $Cu_{46}Zr_{54}$, respectively. Therefore, we make very fine grids with grid spacing (R_g = 0.76 Å) about five times smaller than R_{nn}. Then, we fill the grid points with atom radius (R_{at}) (1.96 Å for Cu, 2.02 Å for Zr, 1.83 Å for Pd, and 1.70 Å for Si). We also fill the empty sites that are close ($R < R_{at} + R_g/2.0$) to more than one atom region, which means filling the empty sites that contain more than one filled nearest-neighbor atoms. This filling procedure is done to ensure no voids are found in the initial structure. Cluster analysis is performed to determine the cluster size based on the grid size.

3. The Voronoi Tessellation Analysis for $Pd_{82}Si_{18}$

To characterize the topological SRO, we use a Voronoi tessellation analysis (25). Here, the indices (n_3, n_4, n_5, n_6) represent the number of i-edge faces of the polyhedron, where the sum of n_i gives the CN of the center atom. The most common Si-centered polyhedra are the tricapped trigonal prism (fraction of 39.6%), corresponding to the index of (0 3 6 0); the deformed icosahedrons (fraction of 26.0%), having the indices of (0 2 8 0); and the standard square dodecahedron (fraction of 3.2%), which has the index of (0 4 4 0).

However, different from Si-centered polyhedral, Pd atoms exhibit over 18 packing-type clusters, where the most abundant ones are (0 3 6 4) (fraction of 11.5%), (0 2 8 2) (fraction of 11.6%), and (0 1 10 2) (fraction of 15.8%).

Although the amount of perfect icosahedra [with index of (0 0 12 0)] is only 5.6%, a noticeable amount of defective or deformed icosahedra form with the indices of (0 2 8 1), (0 2 8 2), and (0 1 10 2). There is also a large amount of crystal-like clusters with (0 3 6 3) and (0 4 4 4) and distorted or defective ones with (0 3 6 4), (0 4 4 3), and (0 4 4 5) that are associated with face-centered cubic- and hexagonal close packed-type structures. The Voronoi analysis on intact $Pd_{82}Si_{18}$ is consistent with a previous study (30).

During the tension process, the main polyhedra remain similar but the ratio changes, as shown in Figs. S2 and S3. Thus, for the Si-centered polyhedra, the (0 4 4 0) type cluster increases abruptly when the tensile strain increased to 0.12.

For the Pd-centered polyhedra, the LCN polyhedra (CN = 8–11) increase. In particular, we find Pd-centered (0 3 6 0) trigonal and (0 4 4 0) dodecahedral clusters that belong to the Bernal holes (26), which will carry large free volume if the center Pd atom is removed.

4. Cavitation-Rate Estimations from Transition-State Theory and MD Simulations

The potential energy (PE) and enthalpy (H) of these LCN-Pd-polyhedra cluster (45 Pd atoms and 5 Si atoms) are −4.03 and −5.35 eV per atom, respectively, whereas the average PE and H for these atoms in the whole system are −4.25 and −5.66 eV per atom, respectively. Because our cavitation events happened at room temperature, we ignore the entropy effects here. Thus, we can estimate the activation energy for this cavitation event is 0.31 eV.

We estimate the surface energy of the critical cavity in Fig. 4*A* by the slab calculation to extract the flat surface energy of 0.973 eV/$Å^2$. Because the cavitation volume is ∼86 $Å^3$, the surface area is estimated to be ∼100 $Å^2$ if we assume a spherical surface. Thus, the surface energy of the critical cavity is estimated to be ∼10.0 eV, which is consistent with the potential energy difference between the clusters and the average of 11.0 eV.

We estimate the prefactors using the previous approach (13), where it is on the order of c_l/L, where c_l is the longitudinal wave speed and L is a cell length of the system. Here, we estimated the c_l/L = 0.56 ps^{-1} by calculating the bulk modulus and shear modulus. Thus, the prefactor is estimated to be 5.0×10^{11} s^{-1}.

To estimate the cavitation time, we need to choose a configuration before ts. Because the time interval between ts and tc is several picoseconds, we estimate the cavitation time is ∼10 ps for the direct MD waiting-time simulation.

5. Fractography of $Cu_{46}Zr_{54}$ Specimens

The fracture surfaces of $Cu_{46}Zr_{54}$ samples was investigated using SEM. The fractograph of a representative $Cu_{46}Zr_{54}$ sample is presented in Fig. S1. As shown, no preexisting pores or inclusions are evident in the fracture surface that could have triggered premature fracture, indicating that fracture was triggered by nucleation of a crack at the core of an operating shear band through cavitation. The left-half region in the fractogram shows evidence of plastic flow consistent with shear band extension, whereas the right-half region shows evidence of smooth facets consistent with crack formation following plastic deformation. This picture supports that shear band extension of ∼0.5 mm (i.e., halfway through the 1-mm sample), followed by crack nucleation through cavitation at the core of an extending shear band.

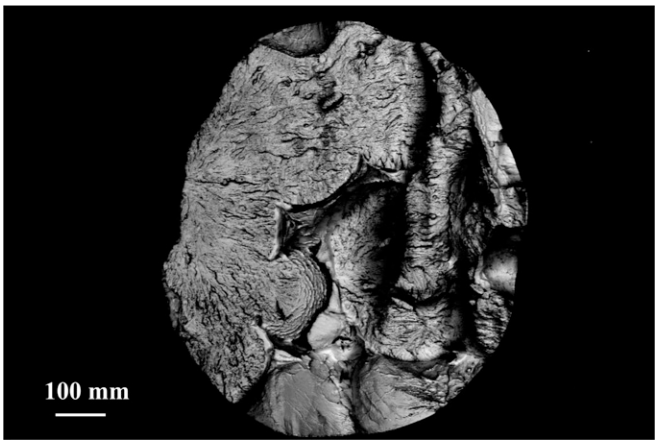

Fig. S1. Fracture surfaces of $Cu_{46}Zr_{54}$ did not reveal presence of any preexisting pores or inclusions that may have triggered premature fracture.

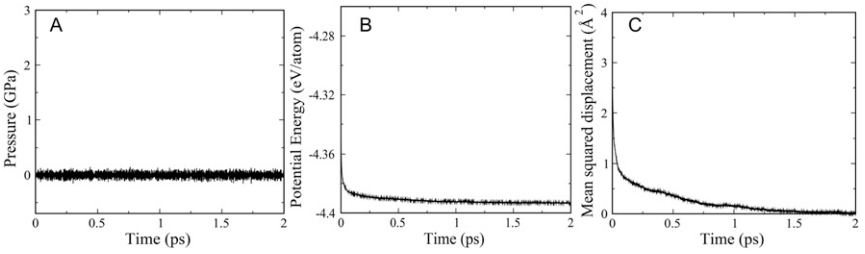

Fig. S2. NPT equilibrium of the structure for 2.0 ns, with 5% exchange of Pd and Si. (*A*) Pressure evolution. (*B*) The potential energy evolution. (*C*) The mean squared displacement of exchanged atoms (the reference is the last snapshot of 2.0-ns NPT dynamics).

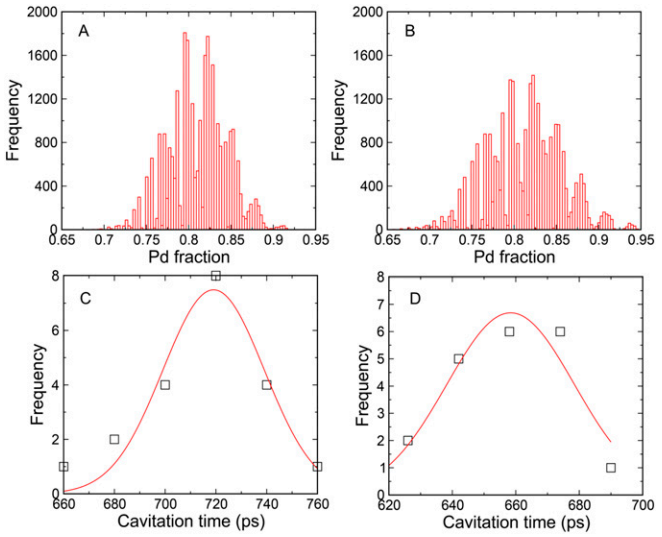

Fig. S3. The Pd distribution in the $Pd_{82}Si_{18}$ system and the corresponding cavitation time fitting by a Gaussian distribution. (*A* and *C*) The original structure where the cavitation time is 719.1 ps. (*B* and *D*) The structure generated by exchange 5% Pd and Si atoms, where the cavitation time is 658.4 ps.

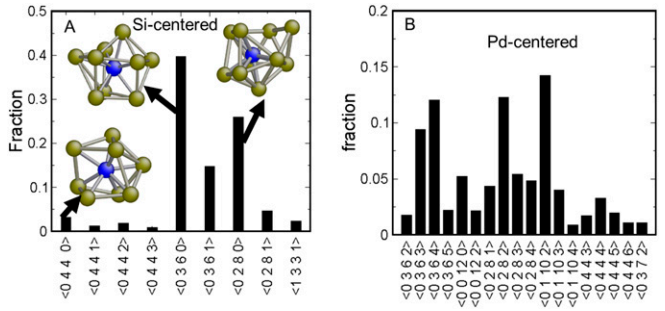

Fig. S4. The Voronoi tessellation analysis for the intact $Pd_{82}Si_{18}$. (*A*) The Si-centered cluster. (*B*) The Pd-centered cluster.

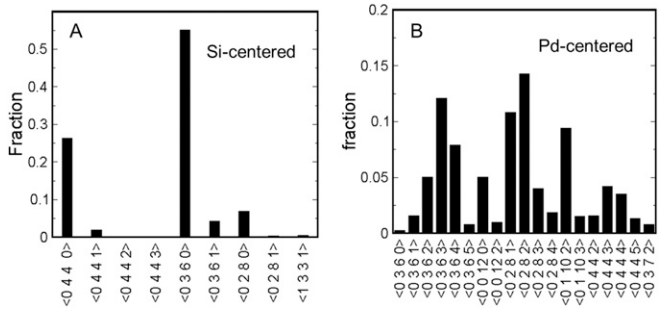

Fig. S5. The Voronoi tessellation analysis for the $Pd_{82}Si_{18}$ at tensile strain of 0.12 before cavitation events. (*A*) The Si-centered cluster. (*B*) The Pd-centered cluster.

Table S1. Statistics of 20 independent cavitation events from tensile deformation

Event	Time 1, ps	Time 2, ps	N_t1*	N_t2†	Vol,‡ Å^3	poly_1§	poly_2¶	poly_3#
1	660	663	3	6	50.3	4	2	0
2	669.5	670	3	8	58.8	4	1	3
3	645.5	646	3	6	64.0	2	3	1
4	647.5	651	3	6	48.7	2	4	0
5	625	656	3	11	102.4	4	5	2
6	676.5	677.5	7	7	59.4	3	2	2
7	634.5	639	4	5	51.8	0	5	0
8	660.5	665.5	2	9	77.7	4	3	2
9	644	648.5	5	9	80.2	1	3	5
10	701.5	705	4	7	88.2	0	4	2
11	684.5	691.5	4	7	48.2	3	0	4
12	642	652	5	5	39.7	2	3	0
13	654	666	2	7	73.7	3	2	2
14	696	698	4	7	47.9	3	2	2
15	670	670	5	5	39.2	1	1	3
16	646	672	3	9	139.0	2	2	5
17	670	670	5	5	56.6	2	1	2
18	692	700	3	4	61.8	1	3	0
19	704	710	3	7	77.9	3	3	1
20	700	704	7	7	86.8	1	2	4

*The number of LCN-Pd-polyhedra at time 1.
†The number of LCN-Pd-polyhedra at time 2.
‡The critical cavitation volume from grid analysis.
§The number of polyhedra with type (0 3 6 0).
¶The number of polyhedra with types (0 4 4 0) and (0 4 4 1).
#The number of polyhedral with others types of (0 5 2 0), (0 5 2 2), (1, 3, 3, 1), etc.

Table S2. Statistics of 7 independent cavitation events from shear deformation

Event	Time 1, ps	Time 2, ps	N_t1*	N_t2†	Vol,‡ Å^3	poly_1§	poly_2¶	poly_3#
1	209	222	1	6	99.9	2	4	0
2	55	58.5	4	7	69.0	1	4	2
3	<50	74.5	<2	8	149.8	2	3	3
4	<110	137.5	<2	5	99.4	1	2	4
5	458	458	10	10	158.0	2	5	5
6	213	233	3	8	88.1	3	0	6
7	66	86	2	6	71.6	2	1	7

*The number of LCN-Pd-polyhedra at time 1.
†The number of LCN-Pd-polyhedra at time 2.
‡The critical cavitation volume.
§The number of polyhedra with type (0 3 6 0).
¶The number of polyhedra with types (0 4 4 0) and (0 4 4 1).
#The number of polyhedral with others types of (0 5 2 0), (0 5 2 2), (1, 3, 3, 1), etc.